Image analysis of petrographic textures and fabrics using semivariance

ANDREW R. H. SWAN AND JANE A. GARRATT

School of Geological Sciences, Kingston University, Penrhyn Road, Kingston upon Thames, Surrey, KT1 2EE, UK

Abstract

Many subjective descriptive terms such as 'smooth', 'coarse' and 'anisotropic' are routinely used to convey properties of textures and fabrics, but these aspects of geological objects are not easily quantifiable. The use of directional semivariograms of image greylevels is assessed for this purpose. These quantify anisotropy of 'coarseness/fineness' by using semivariogram ranges, and 'roughness/smoothness' by using semivariogram sill values. These can be summarized by ellipses derived from semivariogram ranges and directions. The method will find applications in analysis of rock thin sections as well as analysis of surface texture of grains and microfossils.

KEYWORDS: image analysis, petrographic textures, fabric, semivariance.

General properties of an image

IMAGES of geological materials may be digitized as arrays of pixel values that contain nearly all of the information available to the human eye. If the image is of a thin section in transmitted light, the pixel values will be determined by the opacity of the material. If the image is of the surface of a grain or microfossil in reflected light, the pixels will have high values (light) or low values (dark) largely according to the positions of shadows which relate to surface topography. In either case, the spatial distribution of pixel values is likely to contain much information of geological interest.

This paper is not concerned with the very specific, localized features of interest (for example, properties of specific mineral grains) but with the general properties of an image. These include attributes that are visually apparent, traditionally used and of considerable importance in geology. Using simple terminology, these attributes are: 1. coarse *vs.* fine; 2. rough *vs.* smooth; and 3. isotropic *vs.* anisotropic.

The expression of these properties on a pixel array and their interpretations can be considered separately:

1. *Coarse vs. fine.* In terms of pixel values on a scale from black to white (greylevels), a description of an image texture as 'coarse' means that similar greylevel values tend to recur laterally on the image only at relatively large distances. In the frequency domain, variance tends to be at low frequencies (though no regularity is implied). The description of 'coarse' is natural and intuitive where this situation occurs in an image of a surface, perhaps of a fossil with widely spaced ribbing. In the case of thin sections, the term 'coarse' may also be used to describe relatively large grain sizes that may cause the low frequency variation of pixel values. The opposite term 'fine' can be used to describe high-frequency textures.

Note that nothing is implied by these terms about the amplitude of the variation, i.e. whether the greylevels vary from black to white or just pale mid-grey to dark mid-grey.

2. *Rough vs. smooth.* Where the term 'smooth' is used to describe a surface, we understand that it has little topography: on an image, this means that there would be little shadowing and the greylevel values would show low variability. In a thin section, the analogous situation is one of homogeneity. A 'rough'

Mineralogical Magazine, June 1995, Vol. 59, pp. 189–196

texture has high variability or amplitude of greylevels. Note that a perfectly smooth image cannot be assessed for the 'coarse *vs.* fine' property.

3. *Isotropic vs. anisotropic*. The most visually striking property of an image is often its fabric: there may be stripes of contrasting greylevel or a systematic orientation of elongate grains. This property can be conceptualized in terms of anisotropy of coarseness and/or roughness. As described above, coarseness and roughness can be assessed in any one profile across the image. If profiles in all directions give the same properties, then the image is isotropic. It is common, however, for different directions to yield different amounts of coarseness; scans of a thin section perpendicular to bedding or parallel to the direction of maximum strain will tend to encounter more frequent fluctuations in greylevel than scans parallel to bedding or perpendicular to the strain direction. Anisotropy in roughness is also possible and indicates that there are distinct stripes of internally smooth textures. This results from banding rather than from grain shape.

History of research

Research in this field builds on contributions from workers in general image processing and from geologists seeking techniques for specific applications. Techniques developed as general image processing applications are exemplified by the influential paper by Haralick *et al.* (1973), whose approach is similar in some ways to the method to be developed here. In Haralick's method, a variety of greylevel statistics are used to characterise textural features; these are derived from M_δ greylevel co-occurrence matrices, based on matches between pixels separated by distance δ. However, this incurs loss of the information on non-exact greylevel similarities, requires considerable processing and yields a rather indirect measure of textural coarseness at any given separation δ. Weszka *et al.* (1976) reassessed these and other descriptors and found that greylevel statistics performed better than Fourier transforms. Davis *et al.* (1979) developed the use of co-occurrence matrices further and incorporated ideas of coarseness and anisotropy in a similar way to that used here. All of these papers are directed towards characterizing textures for classification; there is no attempt to derive a small number of efficient, concise descriptors.

A further development in textural analysis focuses on the recognition, characterization and relative positions of textural elements. This is exemplified by Tomita *et al.* (1982), whose technique is close to Fry's (1979, see below) method in concept and application.

A different approach involving fractal analysis was used by Peleg *et al.* (1984) in analysing images of a variety of natural textures. Although a fractal dimension is calculable for any image, it is not an efficient descriptor unless the image has genuine fractal properties. An image, for example, of a thin section of sandstone or granite is more likely to be dominated by characteristic grain sizes: these will not induce the properties of scale-invariance for which fractal dimensions are concise descriptors.

Initial work on analysis of anisotropy in rock thin sections was dominated by attempts at deriving strain ellipses on the basis of grain shapes. These methods were summarized by Ramsay and Huber (1983) and include R_f/ϕ methods (Lisle, 1985) and the Fry methods (Fry, 1979; Hanna and Fry, 1979; Erslev, 1988). These approaches are very specific to cases where grains are well defined, grain centres can be found and the objective is restricted to obtaining an estimate of strain. Early work on soils by Smart (1966), and recently developed by Bai *et al.* (1994), assessed anisotropy of grain optical orientation using indices based on the frequency of grains in each of four directional classes, as obtained by using various orientations of polarizers. Such indices have specialized uses but have an uncertain relationship with general rock properties.

Recently, there has been a phase of interest in the analysis of anisotropy of soil and rock images using Fourier and autocorrelation transforms. Derbyshire *et al.* (1992) used the standard 2D Fourier transform applied to SEM images of loess. The ellipticity and oblateness of the anisotropy were derived from contours on the 2D energy spectrum. Similarly, ellipticity of contours of the 2D autocorrelation function was used by Pfleiderer *et al.* (1993) to quantify anisotropy of petrographic images (for application see Pfleiderer and Halls, 1993). These methods are directed at the same properties of anisotropy of coarseness as are investigated in this paper, and, indeed, the autocorrelation approach is closely related mathematically to the semivariance method to be developed here. However, these Fourier and autocorrelation methods involve uncertainties as to which contour should be used to represent the anisotropy, and neither seeks to separate anisotropy of coarseness from anisotropy of roughness ('stripiness').

Semivariance

In order to quantify the conceptual descriptors of image texture and fabric described above, a method is needed that can be applied to individual profiles, which can give estimates of variability (roughness) and which is capable of comparing greylevels at pixels with specified spatial separation (for coarseness). These criteria are met by the procedure of

calculating semivariance: this forms the basis of the technique to be described here.

Semivariance is defined by the standard equation:

$$\gamma_h = \frac{1}{2(n-h)} \sum_{i=1}^{n-h} (x_i - x_{i+h})^2 \qquad (1)$$

where:

γ_h is the semivariance for lag distance h;

x_i is the value (in this study, the greylevel) of the i^{th} data item (pixel) in a profile;

n is the number of data items in the profile.

The semivariance is calculated for all possible integer values of the lag distance h. The equation is based on the sum of the squared differences between the values of all pairs of points that are a distance h apart. The result is shown as a graph of γ_h against h known as a semivariogram (Fig. 1). The semivariance for $h = 0$ must be 0, but the graph typically climbs steadily to higher γ_h with higher h, indicating that points further apart tend to be more dissimilar. Eventually, a value of h is normally reached at which the graph levels out: this value of h is known as the range and the value of γ_h at this plateau is known as the sill value. For any distance h outside the range (i.e. at which the sill value of γ_h applies), the semivariance is not affected by the effect of similarity due to closeness; it is only the result of the overall variability of the data. In fact, it can be shown that the sill value of γ_h is equal to the variance s^2 of the sample of n data values.

Data sequences with rapid, high frequency fluctuations have short semivariogram ranges, as pairs of points even a short distance apart will be unrelated. If data have fluctuations tending to be at longer wavelengths, the semivariogram range will be larger: we would find γ_h remaining less than s^2 at relatively larger values of h.

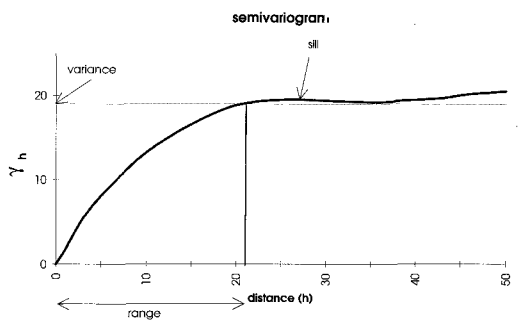

FIG. 1. A typical semivariogram, showing how the semivariance γ_h varies with distance h, and the standard terminology of sill and range. The 'plateau' value of γ_h is the sill value and normally approximates to the variance.

Semivariance was devised in response to problems of estimation of grade of gold ore in South African mines, and is a key element of geostatistics (*sensu* Matheron, 1963). The discipline of geostatistics was developed in response to the realisation that gold ore grade (and many other geological properties) is not distributed randomly in space, but neither is it describable by a geometric function. Attributes having this property are called regionalized variables, and it is contended here that greylevel values on an image of a rock thin section can very often be regarded as such. The semivariogram is an optimal descriptor of the properties of a regionalized variable and should be the preferred method of analysis in such cases. Regionalized variables often contain a component of drift: this is the geostatistical term for a significant linear or polynomial trend. Drift prevents the semivariogram from reaching a level sill value: a linear drift, for example, will cause a continuous increase in γ_h with h. This complicates analysis, and drift is normally removed prior to calculation of semivariance.

In gold grade estimation, the semivariogram is used to characterise the nature of spatial variation of grade so as to produce estimates at unknown points. In the present context, the semivariogram is to be used in an analogous way for characterization of greylevel variation, but estimation is not a requirement. It is common practice in geostatistics to assess the anisotropy of semivariance; see, for example, Bardossy and Bardossy (1984). Semivariograms calculated for various directions are used to calculate an ellipse which describes the range in two dimensions.

Application to rock thin sections

The semivariogram can be used to quantify all of the properties of textures and fabrics that were described in concept in the first section of this paper: coarse *vs.* fine: quantified by the semivariogram range; and rough *vs.* smooth: quantified by the sill semivariance (= variance).

Anisotropy is definable from directional semivariograms. It may be reducable to an ellipse, which allows quantification as: 1) length (representing range or variance) of long axis; 2) axial ratio; 3) direction of long axis.

In detail, the procedure is as follows:

1. Select the desired block of pixels from the image. This should be square (to allow equal opportunity of detection of variability in each direction), but can be of any size, depending on the scale of the texture being investigated and the permissable processing time. We will use m to denote the number of pixels along a side of the square array.

2. Some pre-processing may be required: an image containing large-scale heterogeneities, perhaps the boundary between two lithologies, may have a drift or trend in greylevel values. This should be removed in advance by using residuals from 1st or 2nd order trend surfaces (see Davis, 1986). In practice, this is not often necessary.

3. Calculate the semivariogram for each of four directions: vertical, horizontal and the two 45° diagonals. If we have an $n \times n$ array of square pixels, with greylevel values given by $x_{i,j}$ (where i is the horizontal coordinate and j the vertical coordinate relative to a top left origin), the modifications to the basic semivariance equation (1) are as follows:

Left–right direction:

$$\gamma_h = \frac{1}{2n(n-h)} \sum_{j=1}^{n} \sum_{i=1}^{n-h} (x_{i,j} - x_{i+h,j})^2 \quad (2)$$

Top–bottom direction:

$$\gamma_h = \frac{1}{2n(n-h)} \sum_{i=1}^{n} \sum_{j=1}^{n-h} (x_{i,j} - x_{i,j+h})^2 \quad (3)$$

Top left–bottom right direction:

$$\gamma_{\sqrt{2}h} = \frac{1}{2(n-h)^2} \sum_{j=1}^{n-h} \sum_{i=1}^{n-h} (x_{i,j} - x_{i+h,j+h})^2 \quad (4)$$

Bottom left–top right direction:

$$\gamma_{\sqrt{2}h} = \frac{1}{2(n-h)^2} \sum_{j=h}^{n} \sum_{i=1}^{n-h} (x_{i,j} - x_{i+h,j-h})^2 \quad (5)$$

The unit of the lag distance h is the pixel, but note that for the diagonal directions (equations 4 and 5), the semivariance calculated using a given value of h is actually the semivariance for distance $\sqrt{2}$h, as we compare pixels offset by h units in the horizontal and vertical directions.

Modifications of these equations could readily be devised for intermediate directions, if more detail or rigour is required.

4. Calculate, for each of the four directional semivariograms, the sill value. Although, in the case of a single profile of a regionalized variable, the sill value equals the variance, the overall greylevel variance of the whole array of pixels can not be used as a sill value in the general case. Stripes of contrasting greylevel cause anisotropy of variance; so, for example, perfectly horizontal black and white stripes would give zero variance in the horizontal directional analysis, but vertical scans would yield a variance equal to the total variance. If there is no spatial 'stripiness', the overall variance can be calculated and used as the sill value. Pervasive anisotropy (e.g. due to pure shear) should not affect variance isotropy.

If there is any degree of 'stripiness', the sill value will be different in different directions and must be found separately for each direction. These directional variances can be found during the semivariance calculation as follows:

Left–right direction:

$$s^2 = \frac{1}{n^2(n-1)} \sum_{h=1}^{n-1} \sum_{j=1}^{n} \sum_{i=1}^{n-h} (x_{i,j} - x_{i+h,j})^2 \quad (6)$$

Top–bottom direction:

$$s^2 = \frac{1}{n^2(n-1)} \sum_{h=1}^{n-1} \sum_{i=1}^{n} \sum_{j=1}^{n-h} (x_{i,j} - x_{i,j+h})^2 \quad (7)$$

Top left–bottom right direction:

$$s^2 = \frac{1}{2\sum_{k=1}^{n-1} k^2} \sum_{h=1}^{n-1} \sum_{j=1}^{n-h} \sum_{i=1}^{n-h} (x_{i,j} - x_{i+h,j+h})^2 \quad (8)$$

Bottom left–top right direction:

$$s^2 = \frac{1}{2\sum_{k=1}^{n-1} k^2} \sum_{h=1}^{n-1} \sum_{j=h}^{n} \sum_{i=1}^{n-h} (x_{i,j} - x_{i+h,j-h})^2 \quad (9)$$

If the variance of greylevel is to be compared between images, it is essential that the thin sections and the optical conditions are prepared similarly. If this condition is not met, it can not be corrected by use of image pre-processing, for example by contrast standardization. This will guarantee similarity of image 'roughness' regardless of any real petrographic differences! However, variations in optical conditions will not normally affect variance anisotropy and semivariance range. An exception is comparisons of images in plane- with crossed-polarized light, where differences in anisotropy will reflect any difference between grain orientation and crystallographic orientation.

5. Find, from each of the four directional semivariograms, the effective range value (r). The range is normally the value of h at which the semivariance reaches the sill value (= directional variance), but in practice the slope of the semivariance curve often declines to near zero as the variance is approached and the point of intersection with the sill is poorly defined. It is

preferable to use a consistently lower value of semivariance, γ_r, to find the effective range. We have used the directional variance divided by a critical F value:

$$\gamma_r = s^2/F_{\alpha=0.05;\ \nu=\infty,\infty} \quad (10)$$

(The use of degrees of freedom ν_1 and $\nu_2 = \infty$ is justified by the very large number of pixels normally involved and the slight change in critical F values with large ν. $F_{\alpha=0.05;\ \nu=\infty,\infty} = 1.46$.)

Hence, the effective range r is the distance having semivariance γ_r such that the F ratio s^2/γ_r is equal to the critical value of F: larger distances will tend to have γ_h insignificantly different from s^2. The value of γ_r can be found by linear interpolation between the two lowest consecutive values of h that have γ_h values that straddle γ_r.

6. Plot the directional variance and range values in polar coordinate form and find the directions and lengths of the major and minor axes of the best fit ellipse. This can be done by the least-squares method used by Erslev and Ge (1990), or by iterative optimisation. In some images, anisotropy may best be described by a non-elliptical geometry, for example an oblate shape may be expected where affected by well-defined layering or banding. More than the basic four directions are needed to distinguish elliptical from non-elliptical shapes. The F_D index of Derbyshire *et al.* (1992) could be used to quantify departures from ellipticity.

Results

We have used as an illustrative example a portion of the image presented by Hanna and Fry (1979): see Fig. 2. This has been chosen because the strain analysis results for this image are well documented, so the results of the current method are, to an extent, testable. However, in the following respects the image is far from ideal:

1. The texture is very coarse: it is possible that spurious anisotropies will occur where the grains are truncated by the edges of the scanned pixel array, and the result may be sensitive to the positioning of these edges.

2. There is no apparent anisotropy of variance in the image; as such, the methods of Derbyshire *et al.* (1992) and Pfleiderer *et al.* (1993) would be likely to

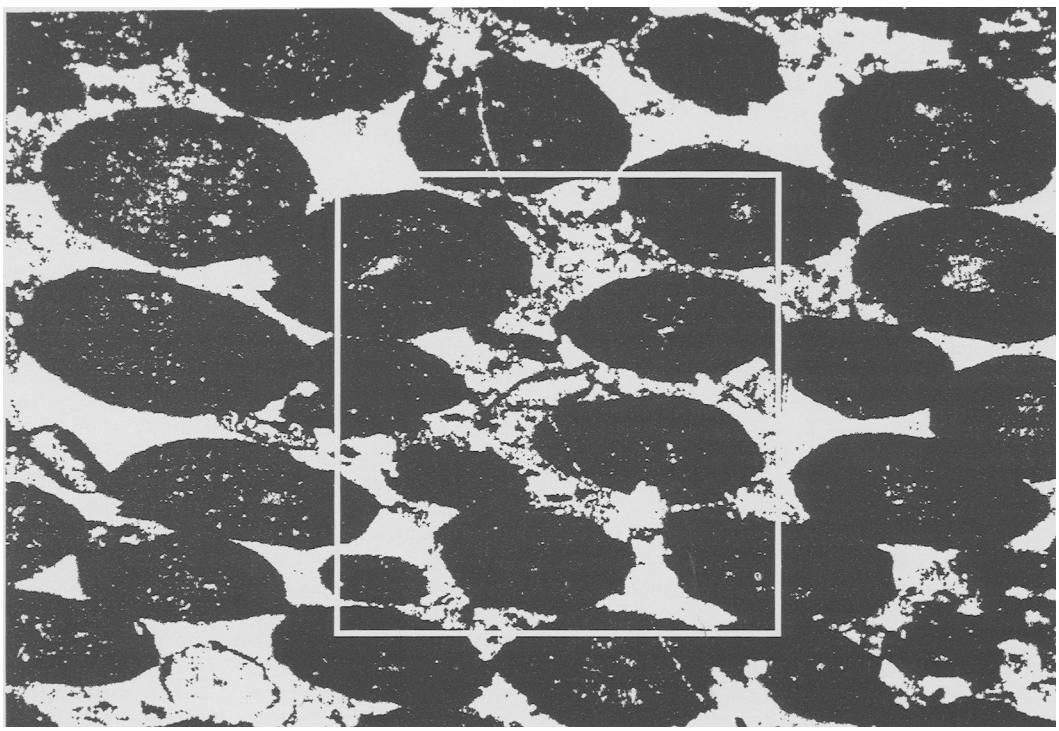

FIG. 2. Scanned version of Figure 1 of Hanna and Fry (1979). The square box delimits the area analysed in this study: the sides have length of 200 pixels (about 1.2 mm in the original rock). The image is reproduced by laser printer with stippled representation of greylevels; this does not reflect the true detail of the analysed image.

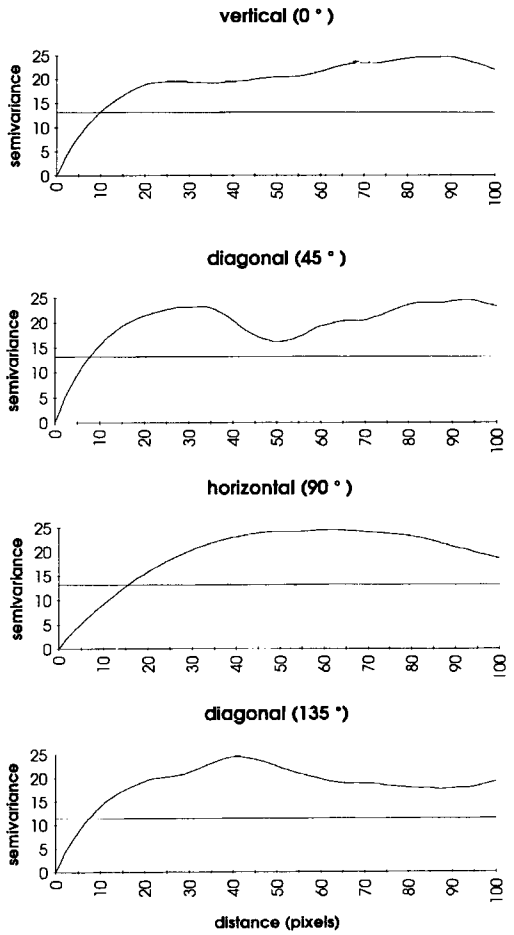

FIG. 3. Directional semivariograms for the image shown in Fig. 2. The horizontal lines give the γ_r values: these intersect the curve to give the range value used here. The horizontal scale for the diagonal semivariograms has units of $\sqrt{2}$ pixels.

obtain the same result with similar efficiency (but, arguably, less rigour).

3. Analysis of visual anisotropy is likely to prove much more useful when the anisotropy is more cryptic: the anisotropy could hardly be more clear in this case!

Furthermore, it should be remembered that anisotropy due to strain is not the only interpretation and application of analysis of visual anisotropy. Results of application to diverse geological contexts will be documented and discussed in a subsequent paper.

Directional semivariograms for the image are shown in Figure 3. The distances (r) at which the semivariance curve crosses γ_r (equation 10) are well defined. The directional variances and effective ranges have been used to define ellipses, shown in Fig. 4.

The directional variance ellipse shows isotropy of 'roughness'. If the image contained any degree of 'stripy' heterogeneity, there would be clear anisotropy of directional variance, with the stripes orientated perpendicular to the long axis of the ellipse. The size of the ellipse (or, in this case, circle) indicates the degree of 'roughness' of the image (variability of greylevels), but this is not an important attribute in this example.

The range ellipse shows a very pronounced anisotropy of 'coarseness': pixels disposed at angles of around 6.5° from vertical tend to become dissimilar at shorter separations than in the perpendicular direction. It is clear that this is due to the shape of the ooids and the anisotropy of the ooid distribution. The ellipse compares well to the ooid orientation and shape, but the strain analysis results documented in Hanna and Fry (1979) give rather larger axial ratios (*c.* 2.4): this appears to be the result of sampling effects: Hanna and Fry base their analyses on more ooids than are shown in their Fig. 1, and that figure is further sub-sampled in our analysis. The size of the range ellipse is directly related to 'coarseness', in this case induced by grain size. However, the precise relationship between semivariogram range and apparent average grain size has not yet been established.

Applications

The new method has performed well in resolving the anisotropy of the chosen image, and has produced interesting, but less testable, results when applied to a wide range of other petrological images (as yet unpublished). Clearly, analysis of anisotropy due to tectonic strain is the obvious application. In the current method (as with those of Derbyshire *et al.*, 1992 and of Pfleiderer *et al.*, 1993), it is not necessary to identify grain boundaries and grain centres, and consequently the method is quicker, more versatile and more rigorous than the Fry and R_f/ϕ methods. It is possible that rough assessments of strain may even be possible using images of suitable field exposures. However, a potential problem is the uncertain relationship between visual anisotropy and strain: images are likely to contain components of anisotropy due to other effects, for example sedimentary layering and metamorphism. It is hoped that these effects may be detectable and separable by analysis of the directional variance ellipse. The separation by the current methodology of pervasive anisotropy from layering or banding has great potential and is not attainable by other methods.

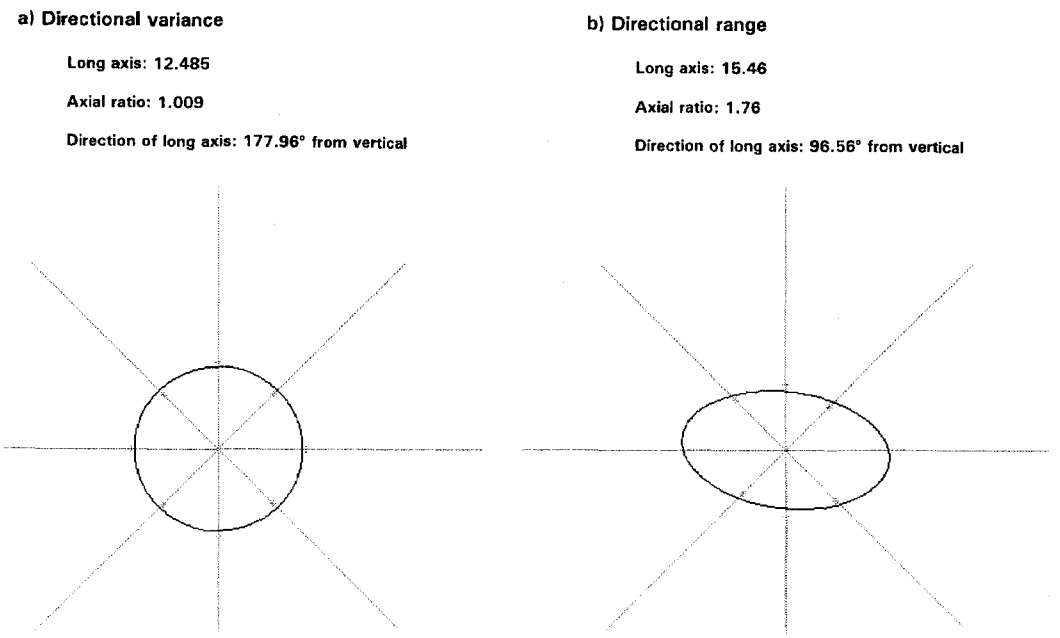

FIG. 4. Best-fit ellipses superimposed on: (*a*) directional variances (units: greylevel^2); (*b*) directional ranges (*r*) (units: pixels). The directional values are shown as crosses on the radiating axes in polar co-ordinate form. The directional variance ellipse shows almost no anisotropy of variance, indicating near isotropy of 'roughness'. The range ellipse shows strong anisotropy, indicating anisotropy of 'coarseness' due to pervasive strain. Compare with the image in figure 2.

Similarly, analysis of visual anisotropy of sediments is likely to yield separable information on sedimentary layering and compaction. Both of these may be correlatable with anisotropy of permeability. In disaggregated sands, the method could be used to quantify grain surface textures (also applicable to microfossils).

As a standard processing tool in an image analysis system, the method will be useful in characterising portions of images. In petrology, the quantification of relief and anisotropy due to cleavage could assist in the diagnosis of minerals.

Acknowledgements

The authors are grateful for the assistance of Phillip Garratt, Darryl Knights and Simon Brandwood. Figure 2 has been reproduced from Hanna and Fry (1979) with kind permission from Elsevier Science Ltd, The Boulevard, Langford Lane, Kidlington OX5 1GB, U.K. We are also indebted to two referees for information and suggestions which have allowed us to correct some important oversights, and to Neil Fortey for encouragement.

References

Bai, X., Smart, P. and Leng, X. (1994) Polarizing microphotometric analysis. *Geotechnique*, **44, 4**, 175–80.

Bardossy, A. and Bardossy, G. (1984) Comparison of geostatistical calculations with the results of open pit mining at the Iharkut Bauxite district, Hungary: a case study. *Mathematical Geol.*, **16**, 173–91.

Davis, J. C. (1986) *Statistics and Data Analysis in Geology*. (2nd Edition). Wiley. 646 pp.

Davis, L.S., Johns, S.A. and Aggarwal, J.K. (1979) Texture analysis using generalized co-occurrence matrices. *IEEE Transactions on Pattern Analysis and Machine Intelligence*, **1**, 251–9.

Derbyshire, E., Unwin, D. J., Fang, X. M. and Langford, M. (1992) The Fourier frequency-domain representation of sediment fabric anisotropy. *Computers Geosci.*, **18**, 63–73.

Erslev, E. A. (1988) Normalized center-to-center strain analysis of packed aggregates. *J. Struct. Geol.*, **10**, 201–9.

Erslev, E. A. and Ge, H. (1990) Least-squares center-to-center and mean object ellipse fabric analysis. *J. Struct. Geol.*, **12**, 1047–59.

Fry, N. (1979) Random point distributions and strain measurement in rocks. *Tectonophys.*, **60**, 89–105.

Hanna, S. S. and Fry, N. (1979) A comparison of methods of strain determination in rocks from southwest Dyfed (Pembrokeshire) and adjacent areas. *J. Struct. Geol.*, **1**, 155–62.

Haralick, R. M., Shanmugam, K. and Dinstein, I. (1973) Textural features for image classification. *IEEE Transactions on Systems, Man and Cybernetics*, **3**, 610–21.

Lisle, R. J. (1985) *Geological Strain Analysis: A Manual for the R_f/ϕ Technique*. Pergamon Press, Oxford.

Matheron, G. (1963) Principles of geostatistics. *Econ. Geol.*, **58**, 1246–66.

Peleg, S., Naor, J. and Avnir, D. (1984) Multiple resolution texture analysis and classification. *IEEE Transactions on Pattern Analysis and Machine Intelligence*, **6**, 518–23.

Pfleiderer, S. and Halls, H.C. (1993) Magnetic pore fabric analysis: verification through image autocorrelation. *J. Geophys. Res.*, **98, B3**, 4311–6.

Pfleiderer, S., Ball, D. G. A. and Bailey, R. C. (1993) AUTO: a computer program for the determination of the two-dimensional autocorrelation function of digital images. *Computers Geosci.*, **19**, 825–9.

Ramsay, J. G. and Huber, M. I. (1983) *The Techniques of Modern Structural Geology. Volume 1: Strain Analysis*. Academic Press, London.

Smart, P. (1966) Optical microscopy and soil structure. *Nature*. **210**, 1400.

Tomita, F., Shirai, Y. and Tsuji, S. (1982) Description of textures by structural analysis. *IEEE Transactions on Pattern Analysis and Machine Intelligence*. **4**, 183–91.

Weszka, J. S., Dyer, C. D. and Rosenfeld, A. (1976) A comparative study of texture measures for terrain classification. *IEEE Transactions on Systems, Man and Cybernetics*. **6**, 269–85.

[*Revised manuscript received 24 October 1994*]